

Resistive switching behavior and mechanism of HfO_x films with large on/off ratio by structure design

Xianglin Huang(黄香林), Ying Wang(王英), Huixiang Huang(黄慧香), Li Duan(段理), and Tingting Guo(郭婷婷)
Citation: Chin. Phys. B, 2024, 33 (**1**): 017303. DOI: 10.1088/1674-1056/ad053a
Journal homepage: http://cpb.iphy.ac.cn; http://iopscience.iop.org/cpb

What follows is a list of articles you may be interested in

Resistive switching properties of SnO_2 nanowires fabricated by chemical vapor deposition

Ya-Qi Chen(陈亚琦), Zheng-Hua Tang(唐政华), Chun-Zhi Jiang(蒋纯志), and De-Gao Xu(徐德高)
Chin. Phys. B, 2023, 32 (**9**): 097302. DOI: 10.1088/1674-1056/acc3fd

Conductive path and local oxygen-vacancy dynamics: Case study of crosshatched oxides

Z W Liang(梁正伟), P Wu(吴平), L C Wang(王利晨), B G Shen(沈保根), and Zhi-Hong Wang(王志宏)
Chin. Phys. B, 2023, 32 (**4**): 047303. DOI: 10.1088/1674-1056/acb421

Digital and analog memory devices based on 2D layered MPS_3 (M=Mn, Co, Ni) materials

Guihua Zhao(赵贵华), Li Wang(王力), Xi Ke(柯曦), and Zhiyi Yu(虞志益)
Chin. Phys. B, 2021, 30 (**4**): 047303. DOI: 10.1088/1674-1056/abd397

Flexible and degradable resistive switching memory fabricated with sodium alginate

Zhuang-Zhuang Li(李壮壮), Zi-Yang Yan(严梓洋), Jia-Qi Xu(许嘉琪), Xiao-Han Zhang(张晓晗), Jing-Bo Fan(凡井波), Ya Lin(林亚), and Zhong-Qiang Wang(王中强)
Chin. Phys. B, 2021, 30 (**4**): 047302. DOI: 10.1088/1674-1056/abc67a

Review of resistive switching mechanisms for memristive neuromorphic devices

Rui Yang(杨蕊)
Chin. Phys. B, 2020, 29 (**9**): 097305. DOI: 10.1088/1674-1056/aba9c7

Resistive switching behavior and mechanism of HfO_x films with large on/off ratio by structure design

Xianglin Huang(黄香林), Ying Wang(王英), Huixiang Huang(黄慧香), Li Duan(段理), and Tingting Guo(郭婷婷)†

School of Materials Science and Engineering, Chang'an University, Xi'an 710061, *China*

(Received 15 July 2023; revised manuscript received 16 September 2023; accepted manuscript online 20 October 2023)

Different bilayer structures of HfO_x/Ti(TiO_x) are designed for hafnium-based memory to investigate the switching characteristics. The chemical states in the films and near the interface are characterized by x-ray photoelectron spectroscopy, and the oxygen vacancies are analyzed. Highly improved on/off ratio ($\sim 10^4$) and much uniform switching parameters are observed for bilayer structures compared to single layer HfO_x sample, which can be attributed to the modulation of oxygen vacancies at the interface and better control of the growth of filaments. Furthermore, the reliability of the prepared samples is investigated. The carrier conduction behaviors of HfO_x-based samples can be attributed to the trapping and de-trapping process of oxygen vacancies and a filamentary model is proposed. In addition, the rupture of filaments during the reset process for the bilayer structures occur at the weak points near the interface by the recovery of oxygen vacancies accompanied by the variation of barrier height. The re-formation of fixed filaments due to the residual filaments as lightning rods results in the better switching performance of the bilayer structure.

Keywords: HfO_x film, resistive switching, structure design, interface modulation

PACS: 73.61.–r, 73.40.Rw, 68.55.–a, 72.20.Jv **DOI:** 10.1088/1674-1056/ad053a

1. Introduction

For decades, great efforts have been devoted to seeking a novel non-volatile memory as the alternative to flash memory since its device size can not be reduced continuously to meet the requirements of portable devices with high storage density, considering the issue of increased leakage current. Recently, much attention has been paid to resistive random access memory (RRAM) as one of the most competitive candidates owing to its merits such as simple device structure, high storage density, and good compatibility with conventional complementary metal-oxide-semiconductor (CMOS) process, in which the resistances can be changed by an external electric field or magnetic field.[1–3] Through the study of a series of switching characteristics, several kinds of switching mechanism for RRAM have been proposed, such as the conductive filament model, space charge limited current effect, Schottky emission, and Poole–Franck effect.[4,5] Although the origin of resistive switching of RRAM device is still under investigation and debate, the significant role of the migration of ions and the redox reactions, which result in formation and rupture of conductive paths in switching layer, on the state of resistances has been widely accepted.[6,7] For binary oxide-based RRAM, migration of oxygen ions leaves an oxygen-deficient region in the film, which is mainly responsible for the resistive switching.[8–10] Research indicates that HfO_x materials have shown some advantages as a promising switching layer for future nonvolatile memory due to their large band gap with high dielectric constant, easily controlled composition, nice scalability, and good switching performance.[11,12] However, similarly to most switching materials, HfO_x-based RRAMs face several challenges in their applications, including random switching behaviors and an ambiguous switching mechanism. A clear understanding of microscopic physical mechanisms is the key point for improving the switching performance. Recently, employing bilayer instead of single-layered switching materials has attracted increasing attention owing to the low power consumption, more stable and controllable resistive switching.[13,14] Methods such as designing bilayer structures or inserting a buffer layer as an oxygen reservoir have been attempted to modulate the defects (mainly oxygen vacancies) in the films or at the interface,[15,16] which would be beneficial to suppressing the random formation of conductive path and to improving the device reliability owing to the modulation of defects. Nevertheless, the switching mechanism and effective method for improving the uniformity and reliability of switching behaviors have been under exploration.

In this work, different device structures of HfO_x/Ti and HfO_x/TiO_x are designed to improve switching performance and understand switching mechanisms of hafnium-based RRAM. The chemical composition and oxygen vacancies of HfO_x-based samples are analyzed by x-ray photoelectron spectroscopy (XPS) technology. The switching characteristics in terms of memory window, distribution of switching parameters, and reliable properties are comparatively investigated. The switching mechanisms are illustrated based on the formation and rupture of oxygen vacancy filaments with the variation of barrier height.

†Corresponding author. E-mail: guott@chd.edu.cn

© 2024 Chinese Physical Society and IOP Publishing Ltd

2. Experimental details

In our experiment, the n^+Si wafers were used as the bottom electrode and soaked in HF solution firstly to remove the oxides at the surface before cleaning, then cleaned by alcohol, acetone, and deionized water sequentially. Then HfO_x films were deposited on Si substrates by radio-frequency magnetron sputtering using an Hf metal target as the source of Hf atoms with O_2 as the reactive gas. During the deposition, the Ar/O_2 was 12/3, the working pressure was 0.3 Pa, and the sputtering power was 70 W. Two different bilayer structures were designed for HfO_x-based memory devices. After the fabrication of HfO_x films, a thin Ti metal layer or TiO_x layer as an oxygen reservoir was deposited on HfO_x films to form HfO_x/Ti and HfO_x/TiO_x(15 nm/5 nm) structures. Ti layer and TiO_x layer were prepared with the gas flux for Ar of 15 SCCM and Ar/O_2 of 15/3, respectively. In addition, single-layer HfO_x films (20 nm) were also fabricated for comparison. All prepared films were post-annealed at 200 °C for 10 min in a nitrogen atmosphere. Finally, the top electrodes of Cu were evaporated with a metal mask to pattern the size to form an MIM structure for measurement. The chemical composition of the films was characterized by XPS technology. The electrical measurements were carried out by an Agilent 4155C semiconductor parameter analyzer using a two-probe method. The voltage was applied on Cu electrode with the Si bottom electrode always grounded.

3. Results and discussion

Figure 1 shows the resistive switching characteristics of HfO_x, HfO_x/Ti, and HfO_x/TiO_x samples. The initial states of the fresh samples are in a high resistance state (HRS) and an electroforming process is required to initiate the switching behavior, as presented in Fig. 1(a). Compared with the HfO_x sample, the forming voltage is reduced by designing a bilayer structure, which may be due to the modulation of defects at the interface. After the forming process, the reversible bipolar switching behavior can be realized by applying the voltage in a counterclockwise direction, as indicated by arrows in Fig. 1(b). The currents increase abruptly at the set voltage, switching the sample from HRS to a low resistance state (LRS). During the reset process, the resistance switches back to HRS. The switching behaviors of HfO_x, HfO_x/Ti, and HfO_x/TiO_x samples are displayed in Figs. 1(b) and 1(d), respectively, and the corresponding cross-sectional TEM images are shown in the insets. The enlarged memory window and much better repeatability of I–V curves can be observed for the HfO_x/Ti and HfO_x/TiO_x samples compared to the HfO_x sample. It is worth noting that the lowest current for all samples is observed at non-zero voltage but the negative voltage. As seen from Fig. 1(b), the minimum current in the HRS of the HfO_x sample is not at 0 V, behaving an open circuit voltage of 0.06 V, which is likely due to the fixed charge or accumulated electrons at the surface of the Si substrate. In addition, the open circuit voltage increases for the bilayer structure, as seen in Figs. 1(c) and 1(d). This phenomenon may be due to the displacement of current and related to the bulk heterojunction composite and the capacitance of the sandwich structure,[17,18] and further investigations are needed.

To analyze the chemical bonding states of the prepared samples, the XPS measurements were carried out. All peaks were calibrated by Au 4f peak (83.8 eV). Figure 2(a) shows the XPS spectrum of Hf 4f in the bulk of HfO_x film, which can be fitted as a double peak of $Hf_{7/2}$ and $Hf_{5/2}$ peaks, corresponding to Hf–O bond.[19] In Fig. 2(b), the O 1s peak in the bulk of HfO_x film can be deconvoluted into two peaks, lattice oxygen with lower binding energy (530.58 eV) and non-lattice oxygen with slightly higher energy (532.28 eV).[20] The concentration of oxygen vacancies is qualitatively estimated by non-lattice oxygen.[21,22] The XPS depth profile of the HfO_x/Ti structure is performed to analyze the O 1s peak near the interface of the HfO_x/Ti structure, as presented in Fig. 2(c). In Fig. 2(c), the fitted result of the O 1s peak is similar to that in Fig. 2(b). The calculated result of oxygen vacancies near the interface of the HfO_x/Ti structure (8.18%) is larger than that in the bulk of HfO_x film (6.72%), which can be attributed to the absorption of oxygen atoms from the HfO_x layer to Ti layer. The inset of Fig. 2(d) shows the XPS spectrum of Ti 2p in TiO_x film. The Ti 2p spectrum can be fitted as a double peak of Ti $2p_{3/2}$ and Ti $2p_{1/2}$ with the binding energies of 458.25 eV and 464.25 eV, in agreement with the reported Ti^{4+}/Ti^{3+}.[23,24] In addition, the oxygen vacancies in TiO_x film (10.27%) are larger than those in HfO_x film, as shown in Fig. 2(d). It can be inferred that the oxygen vacancies near the interface of the HfO_x/TiO_x structure can be modulated as well.

Figure 3(a) shows the distributions of switching voltages for HfO_x, HfO_x/Ti, and HfO_x/TiO_x samples. Compared to the HfO_x sample, better distributions of V_{set} and V_{reset} can be obtained for HfO_x/Ti and HfO_x/TiO_x samples. However, no obvious reduced switching voltages are observed for the bilayer structure, except for the reset voltage of the HfO_x/Ti sample, which may be due to the formation of an interfacial layer although more oxygen vacancies are created near the interface. Since defects can be produced by a higher operating current which is the primary source for the device breakdown,[14] the variations of reset currents are also studied, as displayed in the inset of Fig. 3(a). As can be seen, decreasing reset current can be observed for bilayer structure samples, particularly for the HfO_x/Ti sample, which is beneficial to the decrease of power consumption. Moreover, the HfO_x/Ti sample exhibits a much-scattered distribution of reset current. The distribu-

tions of resistances in LRS and HRS for all samples are presented in Fig. 3(b). Excellent uniformity of resistances can be observed for HfO_x/Ti and HfO_x/TiO_x samples compared to the HfO_x sample. Furthermore, the memory window also improves greatly (>100) by designing the bilayer structure, which mainly results from the increasing resistance in HRS and may be related to the formation of an interfacial layer in the bilayer structure. Compared to the similar research,[25,26] a larger memory window and smaller switching voltages can be observed, indicating a promising application in the future.

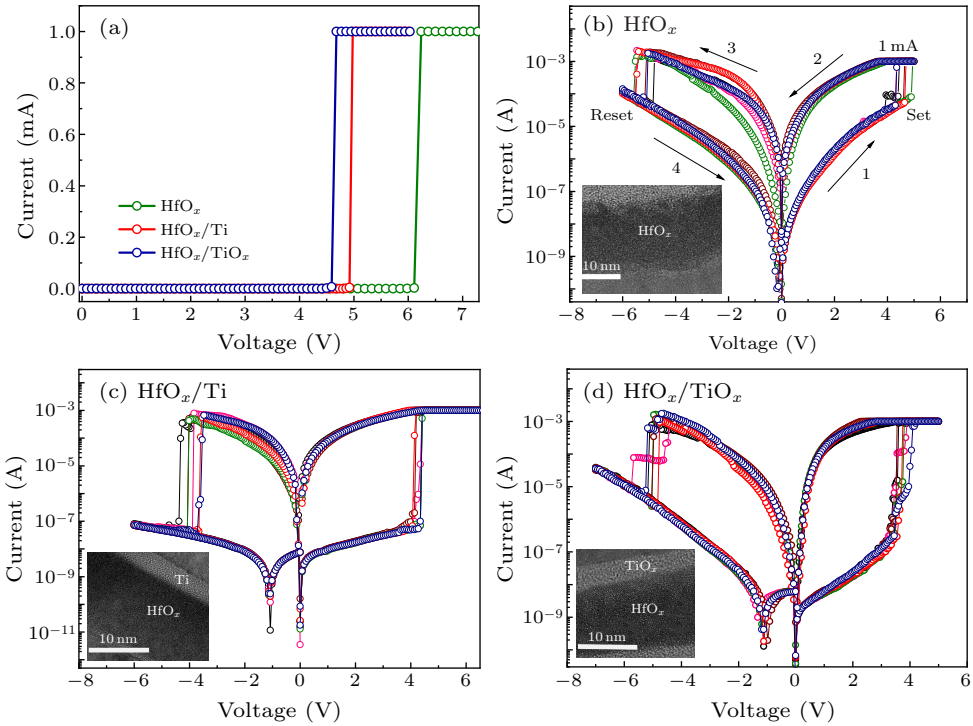


Fig. 1. (a) The forming process of the prepared samples and the typical *I*–*V* curves of (b) HfO_x, (c) HfO_x/Ti, and (d) HfO_x/TiO_x samples. The insets in (b), (c), and (d) show the cross-sectional TEM images of HfO_x, HfO_x/Ti, and HfO_x/TiO_x samples, respectively.

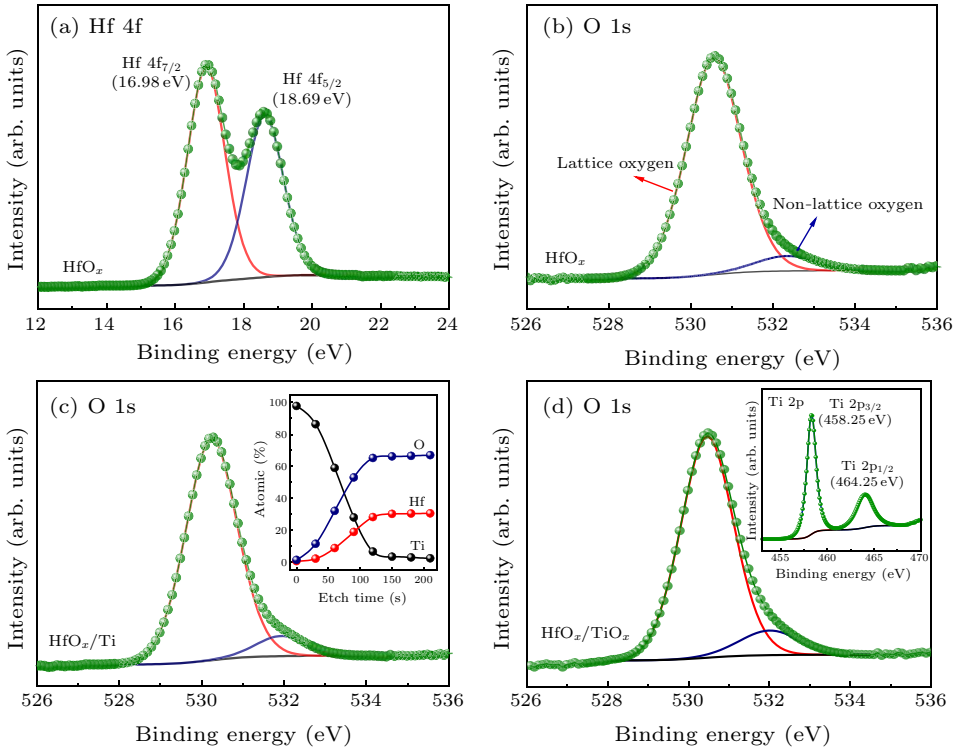


Fig. 2. The XPS spectrum of (a) Hf 4f and (b) O 1s in HfO_x film, (c) O 1s near the interface of the HfO_x/Ti structure, and (d) O 1s in TiO_x film. The inset of (c) shows the XPS depth profile of the HfO_x/Ti structure. The inset of (d) shows the XPS spectrum of Ti 2p in TiO_x film.

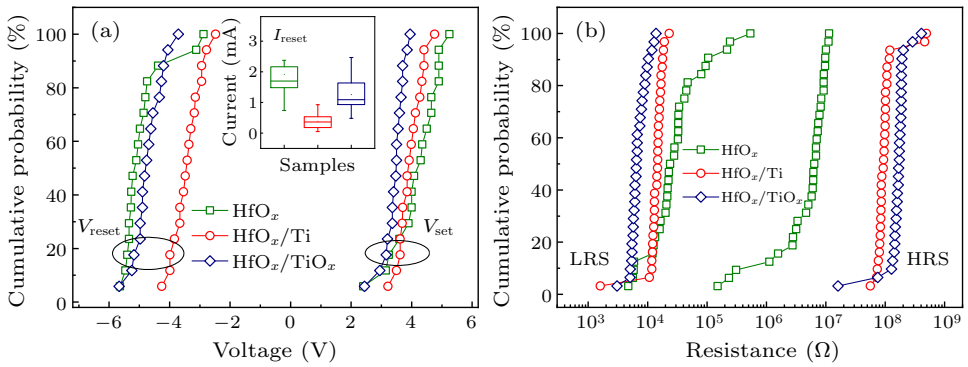


Fig. 3. The distributions of switching parameters of HfO$_x$, HfO$_x$/Ti, and HfO$_x$/TiO$_x$ samples: (a) switching voltages, (b) resistances. The inset of (a) shows the corresponding distribution of reset current.

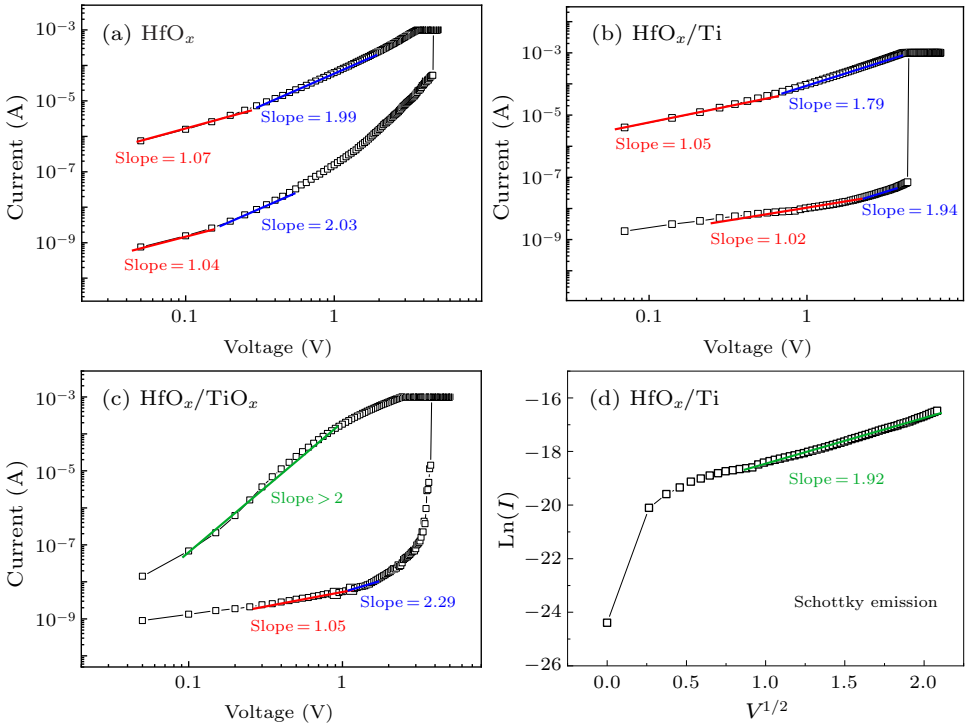


Fig. 4. The fitted I–V curves of HfO$_x$, HfO$_x$/Ti, and HfO$_x$/TiO$_x$ samples.

To explore the current conduction mechanism of the prepared samples, the corresponding I–V curves are replotted and fitted in a double-log scale, as displayed in Figs. 4(a)–4(d). For the LRS of the HfO$_x$ sample, the current and voltage can be fitted as a straight line with a slope of about 1 in a low-voltage region, as shown in Fig. 4(a), exhibiting ohmic conduction behavior. In the high-voltage region, the current is proportional to the square of the voltage, following Child's law. For HRS, the conductive mechanism is slightly complicated and includes three regions: slope ~ 1 at low voltage, slope ~ 2 at higher voltage, and the current increased abruptly with the increased voltage (slope > 3) due to the formation of conducting paths in the switching layer. Such carrier conduction behaviors can be well understood by the SCLC effect,[4,27,28] and are attributed to the trapping and de-trapping process of defects in the film, which are most likely associated with the oxygen vacancies. Similar fitted results can be observed for HfO$_x$/Ti and the HRS of HfO$_x$/TiO$_x$ samples, as presented in Figs. 4(b) and 4(c). However, it is found that the region of abruptly increasing current at high voltage can not be observed for the HRS of the HfO$_x$/Ti sample. Other possible conduction mechanisms have been attempted, and the curve of the HfO$_x$/Ti sample in HRS can be well fitted by Schottky emission, which was an interface-related mechanism, as indicated in Fig. 4(d). The higher barrier height may lead to a larger memory window. Moreover, it is observed that the results of the fitted I–V curve in LRS for the HfO$_x$/TiO$_x$ samples are also different and the slope is much larger (in Fig. 4(c)), which may be ascribed to the fact that partial traps are unfilled and the current density of unfilled ones varies more steeply with the voltage,[29] and the further investigation is required. Overall, the formation and rupture of oxygen vacancy filaments are responsible for the switching behavior of HfO$_x$-based memory.

To further investigate the reliability of the prepared sam-

ples, the endurance and retention properties are demonstrated, as presented in Figs. 5(a) and 5(b). In Fig. 5(a), large fluctuations are observed for the HfO_x sample during switching cycles, which may be related to the random formation of oxygen vacancies during fabrication, and the least memory window is only 10. Better cycling characteristics can be observed for HfO_x/Ti and HfO_x/TiO_x samples, in which the resistances in two states can steadily switch over 120 cycles with the on/off ratio larger than 10^4, mainly attributed to the higher off states due to the higher barrier heights suppressing the electron leaps. Results show some performance advantages of our samples especially in on/off ratio by comparing with other similar bilayer-structured devices.[30–33] Good retention properties can be observed for all prepared samples, as displayed in Fig. 5(b). The currents in LRS and HRS can maintain for 10^4 s without obvious degeneration, showing the non-volatile property of the samples.

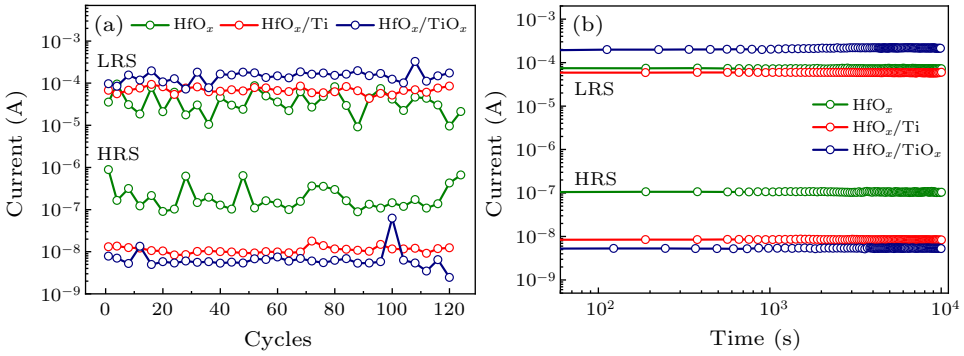


Fig. 5. (a) Endurance and (b) retention properties of HfO_x, HfO_x/Ti, and HfO_x/TiO_x samples. The read voltage was at 1 V.

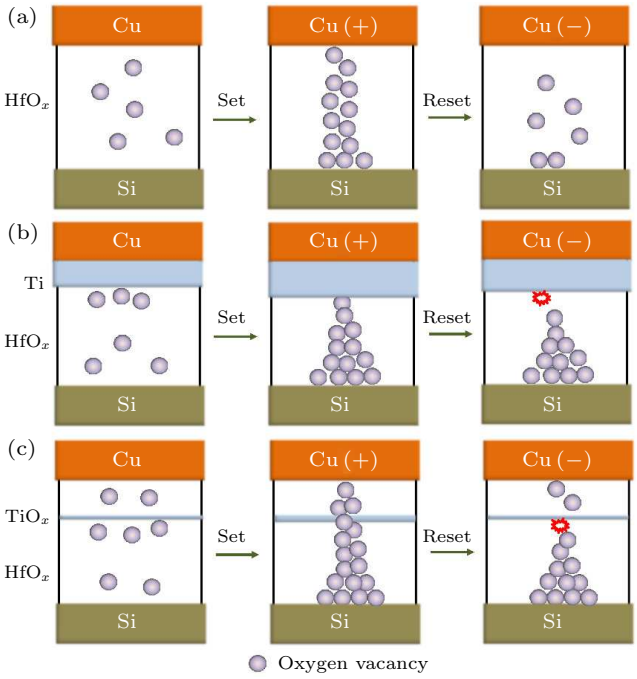


Fig. 6. The physical model of (a) HfO_x, (b) HfO_x/Ti, and (c) HfO_x/TiO_x samples.

Based on the above analysis, the physical models of the switching behaviors of HfO_x, HfO_x/Ti, and HfO_x/TiO_x samples are proposed. For HfO_x samples, the movement of oxygen ions towards the anode under positive voltage leads to the creation of oxygen vacancies which form the oxygen vacancy chains connecting the top and bottom electrodes, assisting the transition of electrons and turning the samples into LRS, as indicated in Fig. 6(a). By applying a negative voltage, the oxygen vacancy chains recovered with oxygen ions, rupturing the conductive paths, and switching the sample back to HRS. Owing to the random formation of oxygen vacancies in the film, the formation and rupture of filaments during each cycle are stochastic, resulting in the poor uniformity of switching parameters.

For the bilayer structure of HfO_x/Ti and HfO_x/TiO_x samples, due to the interface modulation, the resistive switching characteristics are mainly dominated by a redox reaction or Joule heat near the interface, and the schematic diagrams are presented in Figs. 6(b) and 6(c). Ti and TiO_x layers can act as an oxygen-reservoir layer. During the set process, the oxygen ions move towards the anode under the driving force of a positive electrical field and left oxygen vacancies in the film, especially creating more oxygen vacancies near the interface of the HfO_x/Ti sample, as shown in Fig. 6(b). The filaments are formed through the accumulation of oxygen vacancies gradually at the set process and then rupture at the weak points near the interface during the reset process. Furthermore, the higher barrier height was achieved during the reset process, which was contributed to the enlarged memory window. For the HfO_x/TiO_x sample, the different filaments are formed in TiO_x and HfO_x films,[34] the asymmetric conductive filaments lead to the weak points near the interface. On the other hand, due to the different dielectric constants of HfO_x and TiO_x, the filaments at the interface may be the weaker ones.[35] Therefore, under the negative voltage, larger currents at the weak point lead to the first rupture of filaments by the recovery of oxygen vacancies, accompanied by Joule heat at the same time, as displayed in the reset process of Fig. 6(c). In addition, for bilayer structure, it is inferred that the filaments are not com-

pletely ruptured during the reset process and the residual filaments can act as lightning rods and promote the re-formation of fixed filaments along the last path during the subsequent set process. Therefore, much uniform and reliable switching performance can be observed for bilayer structure, which is consistent with Huang' study that the heterostructure and its interface can improve the switching behaviors in multilayer structures.[20] Overall, the results indicate the improvement of switching performance by designing the device structure.

4. Conclusions

In summary, better switching performance including a larger on/off ratio ($\sim 10^4$), uniform distribution of switching parameters, and lower reset current is obtained in the bilayer structures, especially in the HfO_x/Ti sample due to the modulation of oxygen vacancies near the interface and barrier height. Different conduction mechanisms of Schottky emission are observed for the HfO_x/Ti sample, which are closely related to the large memory window and the uniform distribution of the switching parameters. A filamentary model is proposed to clarify the switching behaviors of HfO_x-based samples. Since the weak points of the filaments near the interface are firstly ruptured by the recovery of oxygen vacancies, the residual filaments can act as lightning rods to promote the re-formation of fixed filaments, and better endurance properties can be observed for bilayer structure. Results indicate that the growth of oxygen vacancy filaments can be better controlled by designing a bilayer structure.

Acknowledgements

This work was financially supported by the National Natural Science Foundation of China (Grant No. 51802025) and the Natural Science Basic Research Plan in Shaanxi Province of China (Grant No. 2020JQ-384).

References

[1] Yoon J H, Kim K M, Song S J, Seok J Y, Yoon K J, Kwon D E, Park T H, Kwon Y J, Shao X and Hwang C S 2015 *Adv. Mater.* **27** 3811
[2] Mahadevaiah M K, Perez E, Lisker M, Schubert M A, Quesada E P, Wenger C and Mai A 2022 *Electronics* **11** 1540
[3] Quiroz H P, Calderón J A and Dussan A 2020 *J. Alloys Compd.* **840** 155674
[4] Hu C, Wang Q, Bai S, Xu M, He D, Lyu D and Qi J 2017 *Appl. Phys. Lett.* **110** 073501
[5] Jiao J L, Gan Q H, Cheng S, Liao Y, Ke S Y, Huang W, Wang J Y, Li C and Chen S Y 2021 *Chin. Phys. B* **30** 118701
[6] Sokolov A S, Jeon Y R, Kim S, Ku B, Lim D, Han H, Chae M G, Lee J, Ha B G and Choi C 2018 *Appl. Surf. Sci.* **434** 822
[7] Chen Y Y, Pourtois G, Adelmann C, Goux L, Govoreanu B, Degreave R, Jurczak M, Kittl J A, Groeseneken G and Wouters D J 2012 *Appl. Phys. Lett.* **100** 113513
[8] Akbari M and Lee J S 2016 *RSC Adv.* **6** 21917
[9] Kim J, Lee K, Kim Y, Na H, Ko D H, Sohn H and Lee S 2013 *Mater. Chem. Phys.* **142** 608
[10] Hu C, Wang Q, Bai S, Xu M, He D, Lyu D and Qi J 2017 *Appl. Phys. Lett.* **110** 073501
[11] Dirkmann S, Kaiser J, Wenger C and Mussenbrock T 2018 *ACS Appl. Mater. Interfaces* **10** 14857
[12] Jiang R, Han Z and Du X 2016 *Microelectron. Reliab.* **63** 37
[13] Li J C, Cui H P and Hou X Y 2018 *J. Alloys Compd.* **752** 247
[14] Kim S, Chang Y F, Kim M H, Bang S, Kim T H, Chen Y C, Lee J H and Park B G 2017 *Phys. Chem. Chem. Phys.* **19** 18988
[15] Wu W, Wu H, Gao B, Deng N, Yu S and Qian H 2017 *IEEE Electron. Device Lett.* **38** 1019
[16] Ismaila M, Abbasb H, Choib C and Kim S 2020 *Appl. Surf. Sci.* **529** 147107
[17] Islamov D R, Gritsenko V A, Cheng C H and Chin A 2014 *Appl. Phys. Lett.* **105** 222901
[18] Gao S, Song C, Chen C, Zeng F and Pan F 2012 *J. Phys. Chem. C* **116** 17955
[19] Sharath S U, Bertaud T, Kurian J, Hildebrandt E, Walczyk C, Calka P, Zaumseil P, Sowinska M, Walczyk D, Gloskovskii A, Schroeder T and Alff L 2014 *Appl. Phys. Lett.* **104** 063502
[20] Huang C Y, Huang C Y, Tsai T L, Lin C and Tseng T Y 2014 *Appl. Phys. Lett.* **104** 062901
[21] Shin J, Kim I, Biju K P, Jo M, Park J, Lee J, Jung S, Lee W, Kim S, Park S and Hwang H 2011 *J. Appl. Phys.* **109** 033712
[22] Yeom S W, Shin S C, Kim T Y, Ha H J, Lee Y H, Shim J W and Ju B K 2016 *Nanotechnology* **27** 07LT01
[23] Lin C C, Liao J W and Li W Y 2013 *Ceram. Int.* **39** S733
[24] Biesinger M C, Lau L W M, Gerson A R and Smart R S C 2010 *Appl. Surf. Sci.* **257** 2717
[25] Mallol M M, Gonzalez M B and Campabadal F 2017 *Microelectron. Eng.* **178** 168
[26] Ryu J H and Kim S 2020 *Chaos Solitons Fract.* **40** 110236
[27] Wang S Y, Huang C W, Lee D Y, Tseng T Y and Chang T C 2010 *J. Appl. Phys.* **108** 114110
[28] Jou S and Chao C L 2013 *Surf. Coat. Technol.* **231** 311
[29] Huang R, Yan X, Ye S, Kashtiban R, Beanland R, Morgan K A, Charlton M D B and Groot C H D 2017 *Nanoscale Res. Lett.* **12** 384
[30] Ismail M, Chand U, Mahata C, Nebhen J and Kim S 2022 *J. Mater. Sci. Technol.* **96** 94
[31] Akbari M, Kim M K, Kim D and Lee J S 2017 *RSC Adv.* **7** 16704
[32] Ye C, Deng T, Zhang J, Shen L, He P, Wei W and Wang H 2016 *Semicond. Sci. Technol.* **31** 105005
[33] Zhou L W, Shao X L, Li X Y, Jiang H, Chen R, Yoon K J, Kim H J, Zhang K, Zhao J and Hwang C S 2015 *Appl. Phys. Lett.* **107** 072901
[34] Kim K, Kim E, Kim Y, Sok J H and Park K 2016 *J. Korean Phys. Soc.* **69** 1798
[35] Chen L, Dai Y W, Sun Q Q, Guo J J, Zhou P and Zhang D W 2015 *Solid State Ionics* **273** 66